

# Cross-Spectral Vision Transformer for Biometric Authentication using Forehead Subcutaneous Vein Pattern and Periocular Pattern

Arun K. Sharma, Shubhobrata Bhattacharya, Motahar Reza, and Bishakh Bhattacharya

arXiv:2412.19160v2 [cs.CV] 3 Mar 2025

**Abstract**—Traditional biometric systems have encountered significant setbacks due to various unavoidable factors, for example, face recognition-based biometrics fails due to the wearing of face masks and fingerprints create hygiene concerns. This paper proposes a novel lightweight cross-spectral vision transformer (CS-ViT) for biometric authentication using forehead subcutaneous vein patterns and periocular patterns, offering a promising alternative to traditional methods, capable of performing well even with the face masks and without any physical touch. The proposed framework comprises a cross-spectral dual-channel architecture designed to handle two distinct biometric traits and to capture inter-dependencies in terms of relative spectral patterns. Each channel consists of a Phase-Only Correlation Cross-Spectral Attention (POCSA) that captures their individual as well as correlated patterns. The computation of cross-spectral attention using POC extracts the phase correlation in the spatial features. Therefore, it is robust against the resolution/intensity variations and illumination of the input images, assuming both biometric traits are from the same person. The lightweight model is suitable for edge device deployment. The performance of the proposed algorithm was rigorously evaluated using the Forehead Subcutaneous Vein Pattern and Periocular Biometric Pattern (FSVP-PBP) database. The results demonstrated the superiority of the algorithm over state-of-the-art methods, achieving a remarkable classification accuracy of 98.8% with the combined vein and periocular patterns.

**Index Terms**—Vision Transformer, Biometric Authentication, Forehead Subcutaneous Vein Pattern, Periocular Pattern, Dual-Channel Multi-Attention.

Arun K. Sharma and Bishakh Bhattacharya, are with Department of Mechanical Engineering, Indian Institute of Technology, Kanpur, India (e-mail: arnksh@iitk.ac.in).

Shubhobrata Bhattacharya is with Advanced Technology Development Centre, Indian Institute of Technology, Kharagpur, India (e-mail: emailshubho@gmail.com).

Motahar Reza is with Department of Mathematics, School of Science, GITAM Deemed to be University, Hyderabad, India. (e-mail: mreza@gitam.edu).

## I. INTRODUCTION

In the evolving landscape of biometric identification, the quest for more secure, reliable, non-contact, and non-invasive technologies has become paramount, especially in the wake of global challenges such as the COVID-19 pandemic [1]. Traditional biometrics like face recognition [2], fingerprint recognition [3], iris recognition [4], [5], hand palm vein [6], hand dorsal vein [7], wrist vein [8], finger vein [9], and multimodal biometrics [10] etc has inherent limitations and vulnerabilities that undermine their efficacy and user acceptance. Among these, facial and fingerprint recognition systems stand out as the most prevalent in commercial and semi-commercial applications due to their non-intrusiveness and ease of use. However, the mask-wearing norms and hygiene concerns have significantly impacted their reliability and acceptance [1], propelling the need for alternative biometric solutions that can offer comparable or superior levels of identification accuracy with no drawbacks associated with full-face or touch-based systems.

In recent decades, the forehead vein pattern recognition [11] has emerged as a promising candidate in this context, offering a novel approach to biometric identification that leverages the unique physiological features of the human forehead. This method not only aligns with the requirements for non-intrusive and touchless hygienic biometric systems but also addresses the challenges posed by facial occlusions. The rationale behind focusing on the forehead as a biometric trait lies in its inherent advantages; for example, the forehead remains largely unaffected by facial expressions and is less likely to be obscured by accessories or hair, providing a stable region for identification. Secondly, the area is easily accessible for imaging, even in the presence of face masks, making it an ideal candidate

for recognition in today's real-world scenario.

Bhattacharya *et al.* [11] has attempted to explore the viability of a contactless and real-time system based on the forehead subcutaneous vein pattern and periocular biometric pattern (FSVP-PBP) as an alternative biometric identification method. It uses convolutional neural network-based feature extraction for the vein pattern and the periocular pattern independently, followed by feature concatenation for final classification. The convolutional-based feature extraction method relies on kernel-based spatial features in the input images, which is highly dependent on the resolution of the input images. Therefore, it may fail to capture the subject-specific structural patterns in the forehead image. Furthermore, if the depth of CNN-based models is significantly increased for better performance [9], the computational complexity increases so high that it raises a question of their deployability for real-time applications. Therefore, to improve the robustness against the illumination and the image resolution, this paper presents an innovative lightweight dual architecture of cross-spectral vision transformer (CS-ViT) with a novel phase-only correlation-based cross-spectral attention (POC-CSA) to capture the subject-specific structural pattern from the vein pattern images. The highlights of the contributions of this work are listed below:

- i) An adaptive Tann-Triggs algorithm has been formulated for the preprocessing of the NIR camera-based images to make the vein patterns prominently visible.
- ii) An innovative dual-architectural framework of CS-ViT is formulated to capture the subject-specific structural information from the raw images of the forehead subcutaneous portion and the periocular portion of the subject. The proposed framework of CS-ViT consists of multi-head cross-spectral attention that leverages the concept of Phase-only correlation (POC) to capture the relative orientation of vein patterns for subject-specific feature extraction.
- iii) The performance of the proposed framework was rigorously evaluated on an extended FSVP-PBP database of 350 subjects under two conditions: (i) with raw FSVP-PBP dataset (no preprocessing) and (ii) with FSVP-PBP dataset preprocessed using the proposed adaptive Tann-Triggs algorithm. The evaluation results prove the superiority of the proposed framework over

state-of-the-art algorithms and make it a new benchmark in the domain of non-touch and secure biometric authentication.

The remaining parts of the paper are organized as follows. Section III provides a brief theoretical background of the transformer computer vision and phase-only correlation. Section IV-B describes the proposed CS-ViT framework. Section V presents the effectiveness of the proposed framework and its comparison with state-of-the-art methods on the FSVP-PBP database of 350 subjects. Finally, Section VI concludes the work.

## II. LITERATURE REVIEW

### A. Review of Vein Pattern Recognition (VPR) based on Approaches

1) *Graph-based VPR*: The graph-based VPR relies on feature extraction based on geometrical properties and spatial structures for pattern recognition. The line-like and/or curve-like models: the repeated line tracking method [12], the maximum curvature point [13], mean curvature [14], and Gabor filter [15] have been successfully adopted for robust and discriminative feature extraction. Additionally, statistical analysis tools like principal curvature [16] and vector grams of maximal intra-neighbor difference [17] have also been applied for discriminative feature extraction. The low contrast distribution and uneven illumination cause these methods to be very unreliable and inaccurate.

2) *Deep Learning-based VPR*: Various researchers have explored the performance of the convolutional neural network (CNN)-based deep-learning models for VPR [9], [18]–[20]. The CNN-based methods have outperformed the manually crafted feature methods in the image classification tasks, however, their performances are very much affected due to the scarcity of sufficient vein pattern datasets. Radzi *et al.* [18] introduced a simplified four-layer CNN with an integrated convolutional-sampling structure, trained on a limited dataset. This network, also used in finger vein recognition [19], yielded significantly lower performance than traditional models, highlighting its unsuitability for small datasets. To enhance CNN-based vein pattern recognition, modifying the network architecture for specific tasks [9], [20], [21] or developing quality-aware models [22] have been explored, showing

significant improvements. Some studies propose using a pre-trained CNN [23] and [24] as a feature extractor, drawing features from the fully connected layer or using minutiae-based pooling. However, these methods suffer from biases due to differences between training and target datasets.

3) *Attention-based VPR*: In recent advances in vein-based biometric recognition, various authors have investigated the use of attention-based modern computer vision models [25]–[29]. Li and Zhang [25] introduced FV-ViT, a variant of vision transformer with regularization added in the MLP head, and reported outstanding performance with EER of 0.042% on FV-USM and 1.033% on SDUMLA-HMT datasets. Qin *et al.* [26] introduces a local attention transformer for a full-view finger-vein pattern recognition system that relies on 360-views captured by a rotating LED-based image acquisition system. Further, Qin *et al.* [28] introduced an attention bidirectional LSTM-based temporal-spatial vein transformer that used LSTM with attention and local attention in the ViT model for temporal and spatial feature extraction in multi-view finger vein patterns. In another work on multi-view finger vein recognition, Zhao *et al.* [27] introduced a Transformer-based model with a vein pattern attention module and integrative feed-forward network that uses a vein mask to extract the features from multi-view efficiently. Further, The study by Albano *et al.* [29] leverages explainable AI to enhance transparency in wrist-vein recognition using Vision Transformer (ViT), demonstrating improved verification performance by focusing on key vein patterns.

## B. Review of VPR based on Modality

1) *Finger vein Pattern*: Over the past ten years, there have been remarkable improvements in the field of single-view finger vein recognition technology. These advancements have been fueled by the noticeable difference in appearance between the finger veins and their surroundings in images. Techniques such as Local Maximum Curvature (LMC) [13], Wide Line Detector (WLD) [30], and Enhanced Maximum Curvature (EMC) [31] have been reported. To enhance feature extraction, SSP-DBFL [32] was introduced, combining two types of input features for more effective learning. With the rise of deep learning in the realm of computer vision,

several scholars have tailored these techniques for better finger vein recognition. One notable example is FV-GAN [33], which employs Generative Adversarial Networks (GANs). Similarly, Song *et al.* [34] introduced EIFNet, a model that excels in merging both implicit and explicit features for improved discrimination. Additionally, inspired by the achievements of Vision Transformer (ViT) [35], Huang *et al.* created the Finger Vein Transformer (FVT) [36], which uses a pyramid structure to extract features at multiple levels.

2) *Hand Dorsal vein Pattern*: In 1985, Joseph Rice invented dorsal hand vein (DHV) pattern recognition, securing the first U.S. patent for this technology [37]. In [38], Cross and Smith advanced the technology with thermographic imaging for biometrics. Subsequent advancements included Lin *et al.*'s thermal image-based recognition in [39] and Huang *et al.*'s high-accuracy local feature matching in [40]. In [41], Li *et al.* applied deep learning to DHV recognition, demonstrating the effectiveness of CNNs. Wang *et al.* in [42] proposed a new DHV imaging device and database, employing DNN models for identity and gender recognition. Advancements continued with Gupta *et al.*'s multi-modal biometric system in [43], integrating DHV with other biometrics. Further, Egorov *et al.* [44] proposed the use of scale-invariant feature transform (SIFT) for the feature extraction for DHV pattern recognition.

3) *Hand Palm vein Pattern*: Numerous literature have been reported for the palm vein recognition [45]–[49]. Kang *et al.* [45] developed a contactless identification method using Mutual foreground LBP (MF-LBP) for texture matching. Lee *et al.* [46] introduced the modified  $2D^2$  LDA method, enhancing classical LDA with matrix representations to address singularity issues in high-dimensional data, and reducing computational demands. Xin *et al.* [47] merged local Gabor histograms with LGPDP and LGXP to improve data discrimination and optimized Gabor filter parameters through image sub-division. Bharathi *et al.* [48] focuses on multimodal biometric system using vascular patterns of the hand such as finger vein and palm vein images. Recently, Horng *et al.* [49] explored palm vein recognition in smartphones using RGB images, marking a significant step toward mobile applications.

4) *Forehead vein Pattern*: Forehead biometrics emerges as a promising, non-intrusive identification

method, offering advantages in hygiene and usability, especially under mask-wearing conditions. Recent studies highlight its potential for high accuracy and reliability, leveraging unique forehead features, despite challenges in environmental variability and algorithm development [11]. This method represents a viable alternative to traditional biometrics, adapting to contemporary needs.

### III. THEORETICAL BACKGROUND

#### A. Transformer in Computer Vision

With the outstanding performance of transformer architecture for various applications in natural language processing, Dosovitskiy et al. [50] demonstrated the encoder block of the transformer to be very efficient for image classification in computer vision applications. The transformer encoder architecture introduced for computer vision applications is called Vision Transformer (ViT). The attention mechanism in the ViT provides the capability of capturing the long dependencies in the flattened sequence of image tokens created by splitting an image into patches of size  $16 \times 16$ . The input image is converted into non-overlapping sequential tokens by splitting the image into patches, followed by flattening it into a linear sequence of patches. This mechanism allows the attention mechanism in the transformer encoder to produce class-specific image features by capturing the contextual information in the sequential dependencies of image patches. The final feature output can be further used with a suitable classifier head to predict the class of the input image.

#### B. Phase-Only Correlation

The Phase-only correlation (POC) has received significant popularity as a powerful tool for image processing to measure the alignment or structural similarity of two images in the frequency domain [51]. Let  $\mathcal{F}(u, v)$  and  $\mathcal{G}(u, v)$  are the Discrete Fourier (DFT) of two images  $f(x, y)$  and  $g(x, y)$ . The cross-power spectrum of the transforms  $\mathcal{F}(u, v)$  and  $\mathcal{G}(u, v)$  is defined in equation (1).

$$\mathcal{P}(u, v) = \frac{\mathcal{F}(u, v) \cdot \mathcal{G}^*(u, v)}{|\mathcal{F}(u, v)| \cdot |\mathcal{G}(u, v)|} \quad (1)$$

where,  $\mathcal{G}^*(\cdot)$  denotes the conjugate of  $\mathcal{G}(\cdot)$ . The POC of the two images is mathematically defined in

terms of inverse discrete Fourier transforms of the cross-power spectrum  $\mathcal{P}(u, v)$  in equation (2).

$$\text{POC} = \mathcal{F}^{-1}(\mathcal{P}(u, v)) \quad (2)$$

where  $\mathcal{F}^{-1}(\cdot)$  denotes the inverse discrete Fourier transforms. From equations (1) and (2), it is evident that POC extracts phase information only and ignores the intensity variations. The phase information encoded via Fourier transforms carries most of the structural and geometrical information of the image, the POC-based transformation has performed very well for image-based identification under uncontrolled lighting conditions. A sample visualization of POC for face images from the same person and images from different persons has been depicted in Fig. 1.

#### C. Tann-Triggs Algorithm

Tan and Triggs [52] introduced a chain of preprocessing techniques to eliminate the effect of illumination variations and transform the near-infrared (NIR) camera-based images into prominently visible patterns. The reflections of the vascular tissues of the veins captured by the NIR camera are mostly vague and invisible because of the luminance effect of the NIR domain. The preprocessing algorithm proposed by Tan and Triggs leverages the concept of the Lambertian Reflectance Model (LRM) that assumes an image to be composed of the reflectance (higher frequency component) and the illumination (lower frequency component). The chain of image processing includes: (i) gamma correction, (ii) difference of Gaussian filter, (iii) contrast equalization, and (iv) normalization.

### IV. PROPOSED METHODOLOGY

The overall block diagram for the proposed methodology is illustrated in Fig. 2. The NIR camera images are cropped and separated into the forehead and the periocular portions using the *Haar Cascade Algorithm* provided by *OpenCV*. The cropped images are passed through an adaptive Tann-Triggs (ATT) algorithm to transform to have prominently visible patterns. Now, the processed images of the forehead and the periocular portions are fed to the proposed CS-ViT framework for subject identifications.

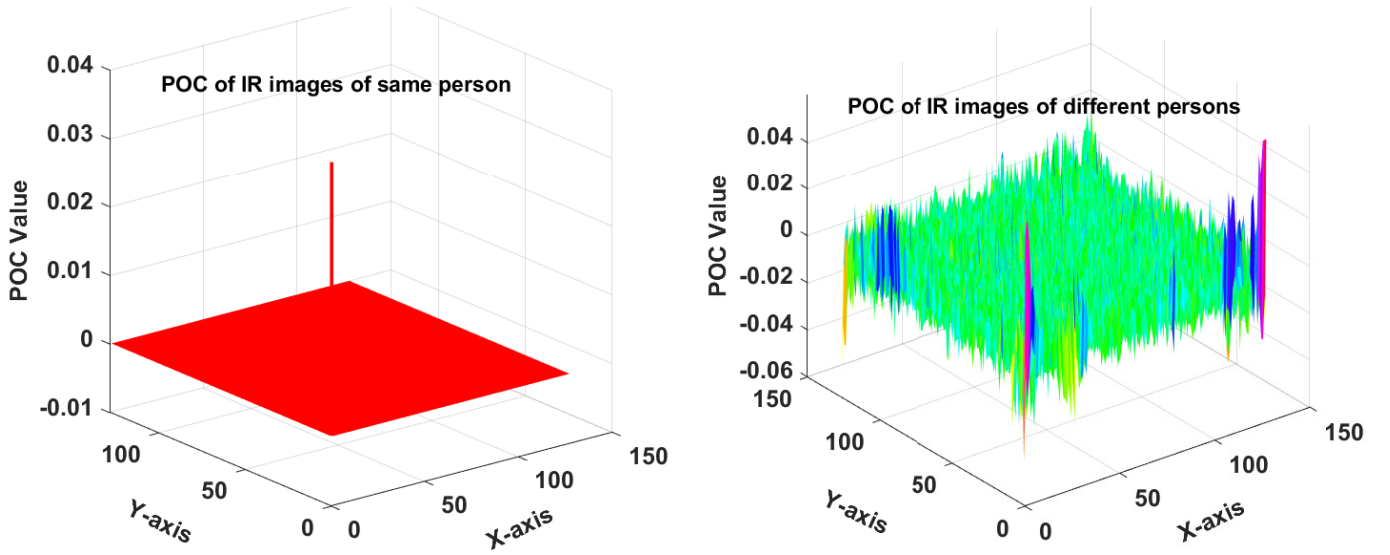


Fig. 1: Comparing the POC-based cross-spectrum vs self-spectrum

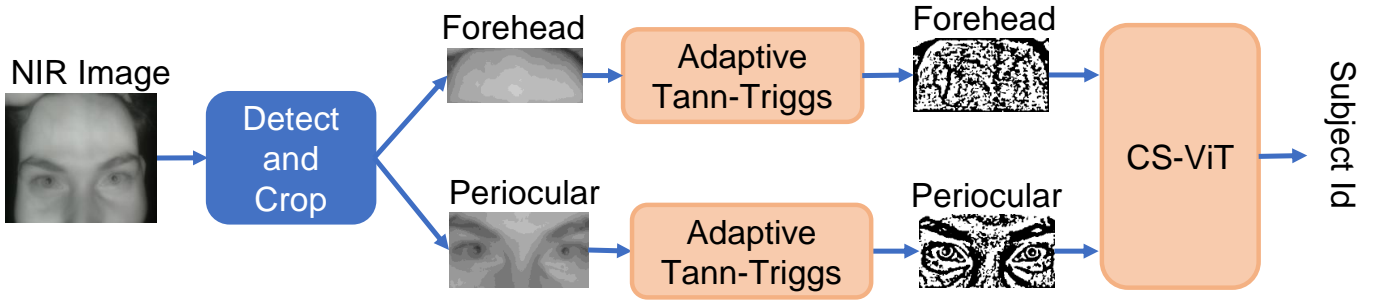


Fig. 2: Complete block diagram of the proposed framework. ATT: Adaptive Tann-Triggs algorithm.

### A. Adaptive Tann-Triggs Algorithm

The original Tann-Triggs algorithm requires suitable tuning of user-defined parameters to get the output image with prominently visible veins. The tuning of these hyperparameters is a time-consuming process or sometimes the manually selected parameters may not produce the desired output. Therefore, this section presents an adaptive Tann-Triggs algorithm that adaptively chooses the hyperparameters based on the image statistics and transforms the NIR image to have prominently visible vein patterns. The chain of the adaptive preprocessing steps is discussed below:

1) *Adaptive Gamma Correction (AGC)*: Adaptive Gamma Correction (AGC) is a gray-level transformation to eliminate the effect of the luminance on the NIR image using the value of  $\gamma_a$ , calculated adaptively based on the standard deviation  $\sigma$  of the normalized image. The gamma-corrected image with adaptive value of  $\gamma$  ( $I_{agc}$ ) is given by equation

(3).

$$I_{agc}(x, y) = I_n^\gamma(x, y) \quad (3)$$

where,  $I_n$  is the normalized image and  $\gamma = \max(0.2, \min(1, 1 - \sigma))$  with  $\sigma$  be the standard deviation of the normalized image, calculated as  $\sigma = \sqrt{\frac{1}{N} \sum_{i=1}^N (I_n(i) - \mu)^2}$ ;  $\mu$  = mean pixel value, and  $N$  = number of pixels.

2) *Adaptive Difference of Gaussian (DoG) filter*: The high-frequency component is further enhanced by applying the difference of Gaussian filters with the adaptively selected kernels  $\sigma_0$  and  $\sigma_1$ , where  $\sigma_1 = 2\sigma_0$  and  $\sigma_0$  is adaptively selected based on the standard deviations of pixel intensities. If  $G_0(x, y)$  and  $G_1(x, y)$  are the Gaussian blurs for  $\alpha_0$  and  $\alpha_1$ , respectively, the DoG filtered image  $I_{DoG}(x, y)$  is obtained as

$$I_{DoG}(x, y) = G_0(x, y) - G_1(x, y)$$

where,  $\alpha_0 = \sqrt{\frac{1}{N} \sum_{i=1}^N (I_i - \mu)^2}$ ; adaptive to the intensity ( $I_i$ ) of the  $i^{th}$  pixel and the mean pixel

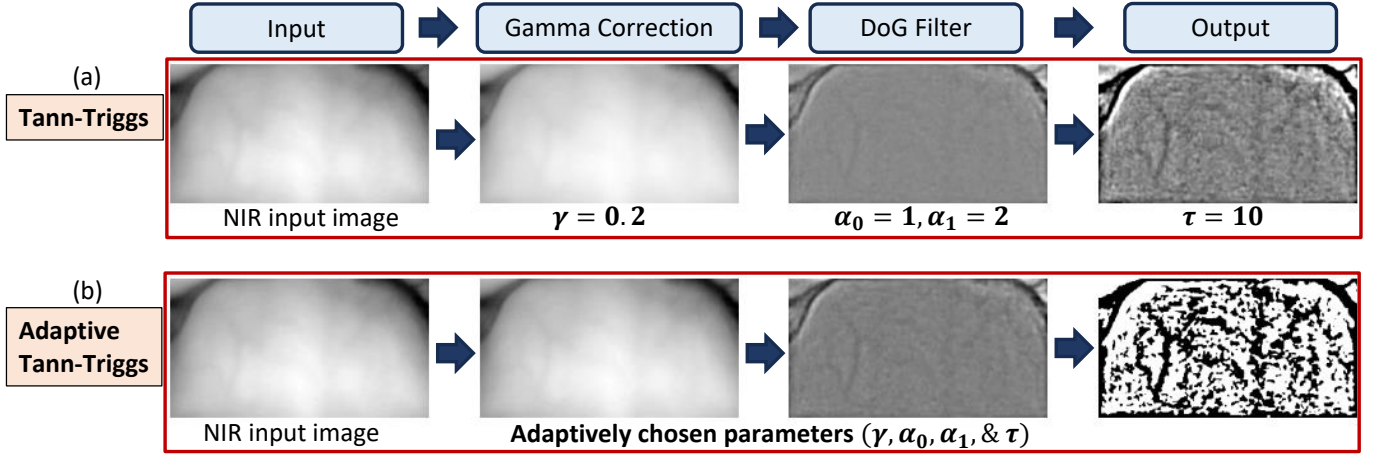


Fig. 3: Comparing the effect of image statistics-based adaptive parameter selection image preprocessing by Tann-Triggs algorithm: (a) Standard Tann-Triggs with user-defined parameters [52] and (b) proposed adaptive Tann-Triggs algorithm with adaptively chosen parameters based on image statistics.

( $\mu$ ).  $N$  be the total number of pixels in the gamma-corrected image. Further details on the computation of Gaussian blur for applying the DoG filter can be found in [52].

3) *Adaptive Contrast Equalization (ACE)*: Now, the uneven/extreme pixel intensity at various portions of the image is suppressed by zero-mean unit variance normalization on the DoG filtered image  $I_{DoG}(x, y)$ , followed by applying a non-linear dynamic truncation as shown in equations (4) and (5).

$$I_z(x, y) = \frac{I_{DoG}(x, y) - \mu_{DoG}}{\sigma_{DoG} + \epsilon} \quad (4)$$

$$I_{CE}(x, y) = \begin{cases} -\tau, & \text{for } I_z(x, y) < -\tau, \\ I_z(x, y), & \text{for } -\tau \leq I_z(x, y) \leq \tau, \\ \tau, & \text{for } I_z(x, y) > \tau, \end{cases} \quad (5)$$

where,  $\tau$  is adaptively selected based on the input image distribution as  $\tau = 1.5\sigma_{DoG}$ ;  $\sigma_{DoG}$  and  $\mu_{DoG}$  are the standard deviation and mean of the  $I_{DoG}(x, y)$ .

The  $I_{CE}(x, y)$  is further normalized to obtain the final enhanced image. The benefit of adaptively selected parameters like  $\gamma$  exponent for gamma correction,  $\alpha_0$  and  $\alpha_1$  for DoG filtering, and  $\tau$  for CE is illustrated in Fig. 3 by comparing the outcomes with the default suggested values in the original paper [52].

### B. Cross-Spectral Vision Transformer

The proposed framework of **Cross-Spectral Vision Transformer (CS-ViT)** comprises  $N$ -

numbers of cross-spectral encoder blocks having dual-channel of multi-head POC-based cross-spectral attention (POC-CSA). The dual-channel of multi-head POC-CSA has been specifically designed to transform the two biometric traits for learning the person-specific signature. The schematic diagram of the proposed framework has been shown in Fig. 4. The two input channels receive flattened patches of NIR camera-based images of the forehead and the periocular portion of faces. Further detailed descriptions of each step are provided in the following sub-sections.

1) *Patch Sequencing*: This step converts the input image to the sequence of token embeddings [50]. The patching step uses 2D convolution to convert the input image to a sequence of 2D patches of size  $(d_p \times d_p)$ . If the resulting number of patches is  $N_{patches}$ , one batch of input images is converted into  $(b \times N_e \times d_p \times d_p)$ , where  $b$  denotes the batch size and  $N_e$  denotes the embedding size or number of patches. Now, each 2D patch in the flattened sequence is converted to 1D sequence of size  $(d_s \times 1)$ , where  $d_s = d_p \times d_p$ . The final flattened patches of shape  $b \times N_e \times d_s$  are the input to each channel of the cross-spectral encoder.

2) *Cross-Spectral (CS) Encoder*: The CS encoder consists of a dual-channel cross-spectral attention mechanism to accept flattened patches of the forehead and periocular channels independently and extract person-specific features. Each channel comprises a multi-head POC-CSA, followed by a non-linear feed-forward block.



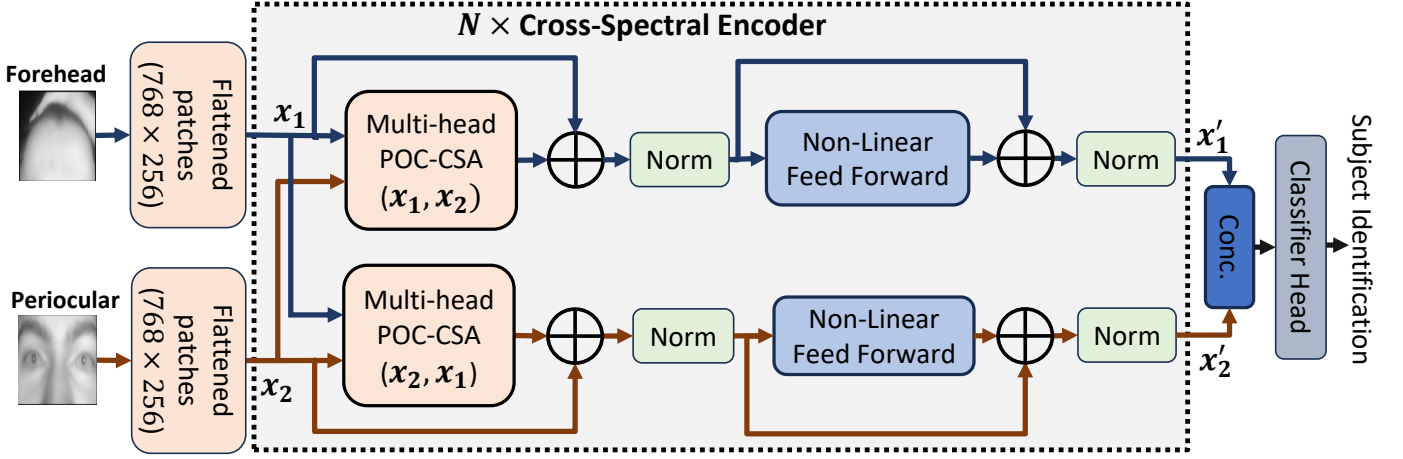


Fig. 4: Proposed framework of cross-spectral vision transformer (CS-ViT) architecture.

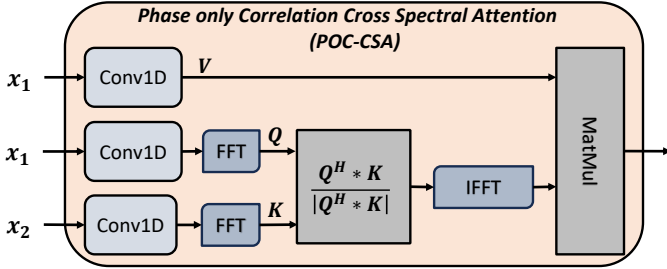


Fig. 5: Schematic diagram of  $\text{POC-CSA}(x_1, x_2)$ , where  $x_1$  = channel input value and  $x_2$  = cross-channel input;  $Q^H$  represents conjugate transpose of  $Q$ .

3) *Multi-Head POC-based CS Attention*: The multi-head POC-based CS Attention block consists of multiple POC-CSA heads in parallel. The basic principle behind POC-based cross-spectral attention is to capture the phase correlation between the two biometric traits and multiply it with the corresponding channel value for a subject-specific transformation. The schematic diagram of a POC-CSA head is shown in Fig. 5. Each head takes three inputs: Query ( $Q$ ), Key ( $K$ ), and Value ( $V$ ). Let  $x_1$  and  $x_2$  represent the inputs to channel-1 and channel-2, respectively. The multi-head POC-CSA in the first channel computes CS attention of  $(x_1, x_2)$ , while the multi-head POC-CSA in the other channel computes cross-spectral attention of  $(x_2, x_1)$ .

For the computation of CS attention of  $(x_1, x_2)$ ,  $V$  and  $Q$  are calculated using  $x_1$ , while  $K$  is calculated using  $x_2$  as shown in equations (6), (7),

and (8).

$$V = f^h(x_1) \quad (6)$$

$$Q = \mathcal{F}(f^h(x_1)) \quad (7)$$

$$K = \mathcal{F}(f^h(x_2)) \quad (8)$$

where  $f^h(\cdot)$  represents 1D convolutional function with kernel size of  $h$  and  $\mathcal{F}(\cdot)$  represents FFT. The convolutional function's kernel size ( $h$ ) is chosen such that  $h \times \text{number of heads} = N_{\text{patch}}$ . The cross-spectrum that represents phase-only information is obtained between  $K$  and  $Q$  as shown in Eq (9).

$$\mathcal{M}_{cs} = \frac{Q^H * K}{|Q^H * K|} \quad (9)$$

where,  $Q^H$  denotes conjugate transpose of  $Q$ . The inverse fast Fourier transform of  $\mathcal{M}_{cs}$  represents the POC between  $Q$  and  $K$ . The obtained POC represents the structural map between the two inputs (the periocular and the forehead vein patterns), which carries unique information about the subject identification. Therefore, the real part of the POC obtained in Eq (9) is termed the attention score and is multiplied by  $V$  to compute the final attention value ( $\mathcal{M}$ ) as shown in Eq. (10).

$$\mathcal{M} = V * \mathcal{R}(\mathcal{F}^{-1}(\mathcal{M}_{cs})). \quad (10)$$

where  $\mathcal{R}(\cdot)$  represents the real part of the complex output of the inverse transform  $\mathcal{F}^{-1}(\cdot)$ . The size of the attention heads is selected such that the concatenated output of the multi-head block is the same as the flattened patch size ( $b \times N_e \times d_s$ ). Therefore, no projection layer is required for combining the outputs of the multiple heads. If  $\mathcal{M}_1, \mathcal{M}_2, \dots, \mathcal{M}_n$

are the outputs of  $n$  number of heads, the final output of the multi-head POC-CSA can be obtained by concatenating along the embedding axis using Eq. (11):

$$\mathcal{M}_o = \text{Concat}(\mathcal{M}_1, \mathcal{M}_2, \dots, \mathcal{M}_n) \quad (11)$$

4) *Feed-Forward Layer*: The output of the multi-head attention block is now added to the corresponding channel input (skip connection) and passed through layer normalization for training stabilization. Now, the normalized output is further transformed by a two-layer feed-forward neural network. The two layers of the MLP block sandwich a non-linear activation layer that adds nonlinearity in the higher-dimensional space. Overall, this block transforms the attention features suitable for final classification.

5) *Classification Head*: Finally, feature outputs from the dual-channel CS encoder are concatenated along the embedding (feature) dimension. The concatenated features are processed by a classifier head designed to transform the feature outputs to the final subject identification. The feature output of each encoder channel has a shape of  $b \times d_h$ . The concatenated features get a shape of  $b \times 2d_h$ . Therefore, the classifier head has the first linear layer with the number of nodes equal to  $2d_h$ , followed by non-linear transformation using a Parametric Rectified Linear Units (PReLU) activation layer, and the last softmax layer having nodes equal to the number of classes or subjects in the dataset.

## V. EXPERIMENTAL RESULTS AND DISCUSSION

### A. Dataset Description

In this study, we prepared an extended version of the Forehead Vein Pattern and Periocular Biometric Pattern (FSVP-PBP) Database [11]. This database contains 25 frames/subjects of the upper face area (eyes and forehead) recorded on 350 subjects (individuals) aged between 21 and 42 years. The images were captured by an NIR camera in a controlled environment with illumination between 20 and 40 Lux in order to reduce the impact of external lighting and effectively capture the LED light reflected off the participants. Subjects were asked to stay within a 4 to 6 centimeter range from the NIR camera during the image collection phase. Prior to the session, individuals were recommended to clean their faces to remove any sweat or oil, ensuring the quality of

the images. Each subject was positioned in front of the camera for about 10 seconds, allowing for the capture of multiple frames.

### B. Training and Evaluation Scheme

The extended FSVP-PBP database contains 8750 images (25 frames/subject) recorded on 350 subjects under variable illumination conditions. The total database is split into training and testing portions with a ratio of 80 : 20 using the random sampling method. The training and validation are performed in the following two cases:

- i) **No Preprocessing**: The NIR image contains noises and vagueness due to the luminance effect in the NIR domain. This poses the requirement of suitable preprocessing to enhance the captured raw images. However, the proposed algorithm leverages the benefit of the POC-based cross-spectral attention mechanism to extract the phase-only information, which is robust to noises due to the luminance effect. The raw images from the training and testing datasets are directly applied to the proposed framework CS-ViT via patch embedding.
- ii) **Preprocessing with Adaptive Tann-Triggs**: To remove the effect of luminance on the NIR images, the raw images are preprocessed using the adaptive Tann-Triggs algorithm, proposed in Section IV-A. The adaptive Tann-Triggs chooses required parameters adaptively based on the statistics of the input image and transforms to prominently visible vein patterns as depicted in Fig. 3(b). The preprocessed images from training and testing datasets are now used for training and validation.

### C. Evaluation metrics

The proposed framework is evaluated in terms of the following evaluation metrics:

- 1) **Classification accuracy (CA)**: Classification accuracy ( $CA$ ) as widely accepted in the literature [53].  $CA$  is defined as

$$CA = \frac{\text{No. of correct predictions}}{\text{No. of test samples}} \times 100\% \quad (12)$$

- 2) The **Equal Error Rate (EER)** is a metric for evaluating biometric system performance, where the False Acceptance Rate (FAR) and



False Rejection Rate (FRR) meet. It balances security (lowering false acceptances) and usability (reducing false rejections), with a lower EER indicating higher accuracy and a more reliable security system.

- 3) The **True Acceptance Rate (TAR)** is the measure of correct identification or legitimate acceptance by the verification systems. TAR @FAR=0.1% is the percentage of correct identification while maintaining very low impostor acceptance (only 0.1% false acceptance of wrong users).
- 4) Training statistics of the models are evaluated in terms of %CA on the training and validation datasets and are presented as training and validation curves with respect to epochs.

#### D. Implementation Details

The proposed CS-ViT as shown in Fig. 4 is implemented using the PyTorch library of Python on the Linux platform. The model's hyper-parameters were selected as follows: number of CS-Encoder blocks = 6, number of heads in multi-head attention blocks = 8, input image size = 256, patch size =  $16 \times 16$ , the embedding dimension = 512, sequence size =  $16 \times 16 = 256$ , and number of hidden sizes for the non-linear feed-forward block =  $2 \times \text{embedding dimension}$ . Therefore, the output of the last encoder at each channel has a shape of  $b \times 256 \times 512$ , where  $b$  represents the batch size. The final output features of each channel are obtained by taking the mean along the sequence dimension (256), which ultimately converts to the shape of  $b \times 512$ . Both feature outputs are concatenated along the feature dimension to obtain a feature size of  $b \times 1024$ .

The concatenated output of the encoder block is passed through a custom classifier, designed to accept input features of size 1024 with one intermediate layer to transform the feature size successively from  $1024 \rightarrow 512 \rightarrow 350$ , where 350 is the number of classes in the dataset. The intermediate layer having 512 hidden nodes is activated using a learnable parametric activation function, called PReLU, described in Section IV-B5.

The weights of the model are initialized using Xavier initialization. The model is trained using the training dataset under the two cases as described in V-A for 200 epochs on the *NVIDIA Tesla V100* GPU at SMSS Lab, Department of Mechanical Engineering, IIT Kanpur. The training statistics curve in

terms of training accuracy and validation accuracy is shown in Fig. 6

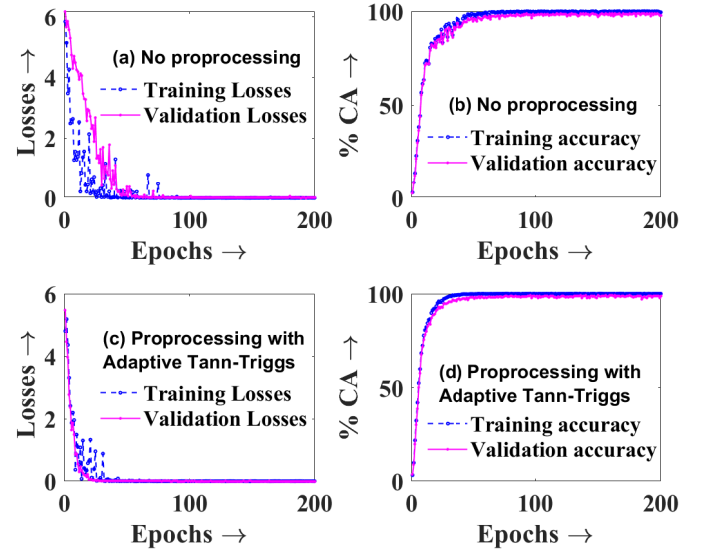


Fig. 6: Training and validation statistical curve for the proposed CS-ViT: (a) training and validation losses

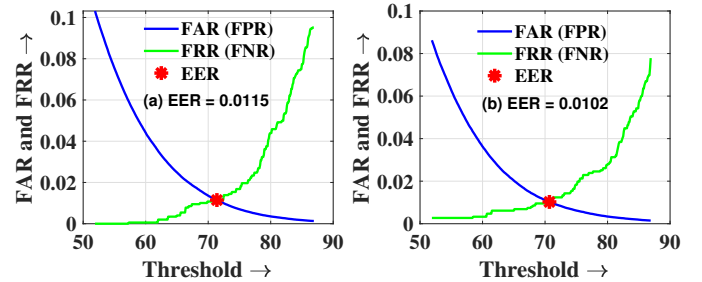


Fig. 7: Computation EER using FAR curve and FRR curve for CS-ViT on the validation data with: (a) no preprocessing and (b) preprocessing by adaptive Tann-Triggs algorithm.

#### E. Comparison with State-of-the-art Methods

For further validation of the proposed framework for biometric authentication, this section presents a comparative analysis of the performance of various algorithms on the aforementioned extended FSVP dataset. The study encompassed a range of recent methods for comparison: VGG-16 [54], ResNet-50 [55], GoogleNet [56], PV-CNN [9], 2D FV-ViT [25], FV-LT [26], VPCFormer [27], and ABLSTM-TSVP [28]. All these algorithms accept single-channel input only, but the FSVP dataset contains forehead vein patterns and particular images captured by the NIR camera. Therefore, images of the two biometric traits (forehead and periocular) were concatenated along the suitable dimension to

make single-channel input for each subject from the train and the test samples. Each model was trained for 100 epochs and evaluated on the test dataset. The performances in terms of CA, EER, and TAR have been presented in Tables I and II for the cases of no preprocessing and preprocessing with the adaptive Tann-Triggs algorithm. It can be observed that the proposed framework demonstrated the highest performance with near-perfect classification, evident from the highest values of CA's and TAR's, and lowest values of EER's in both cases. The comparison of the results by the proposed framework under the two cases in Tables I and II reveals that the POC-based cross-spectral attention mechanism is sufficiently robust to capture the structural pattern from the NIR camera-based raw images. However, the application of the adaptive Tann-Triggs algorithm for preprocessing the vein patterns marginally enhances the performance of the proposed CS-ViT framework. Very low EER value and high TAR signify that the proposed model offers a highly reliable security system with a very low failure rate and high acceptance of legitimate users only.

Table I: Performance comparisons for the dataset with no preprocessing

Method	Accuracy	EER	TAR @FAR=0.1%
VGG16 [54]	91.6	2.512	58.40
ResNet50 [55]	92.7	1.806	82.60
GoogleNet [56]	93.5	0.986	78.80
PV-CNN [9]	88.8	2.370	62.05
2D-FV-ViT [25]	94.6	1.875	87.60
FV-LT [26]	95.0	1.056	90.60
VPCFormer [27]	96.8	0.984	95.50
ABLSTM-TSVT [28]	96.4	0.950	97.50
<b>CS-ViT (Proposed)</b>	<b>98.3</b>	<b>0.012</b>	<b>97.80</b>

#### F. Comparison with State-of-the-art Methods with other Biometric modalities

The proposed CS-ViT framework for biometric authentication, trained on the extended database of the FSVP-PBP dataset having 350 subjects, demonstrates superior performance in comparison to state-of-the-art (SOA) biometric systems trained on the

Table II: Performance comparisons for the dataset with preprocessing using adaptive Tann-Triggs

Method	Accuracy	EER	TAR @FAR=0.1%
VGG16 [21]	94.3	2.512	58.40
ResNet50 [55]	94.5	1.806	82.60
GoogleNet [56]	95.5	0.986	78.80
PV-CNN [9]	90.3	2.370	62.05
2D-FV-ViT [25]	95.34	1.875	87.60
FV-LT [26]	97.5	1.056	90.60
VPCFormer [27]	98.0	0.984	95.50
ABLSTM-TSVT [28]	97.5	0.950	97.50
<b>CS-ViT (Proposed)</b>	<b>98.8</b>	<b>0.010</b>	<b>98.50</b>

same dataset. The CS-ViT model achieves a classification accuracy of 98.8% and a very low EER of 0.010, significantly outperforming other methods. For instance, the dual-channel convolutional neural network (DCNN) approach on the same database achieves a classification accuracy of 88.80% and an EER of 2.370, indicating the enhanced precision of the proposed framework. Other biometric systems, such as those utilizing finger vein patterns (FVP), dorsal hand vein patterns (DHVP), and dynamic palm vein matching (DPVM), exhibit lower classification accuracies and higher EERs, as summarised in Table III. For example, the DPVM method on the PolyU database achieves a classification accuracy of 95.59% with an EER of 0.08, while another DPVM method on the CASIA database achieves an EER of 0.12. Furthermore, multimodal systems combining various patterns, such as iris and periocular patterns (IP+PBP), sclera and periocular patterns (SRP+PBP), and palm print with dorsal hand vein patterns (PPP+DHVP), also fall short in comparison. The IP+PBP system achieves a classification accuracy of 93.50% with an EER of 15.50, and the PPP+DHVP system achieves a classification accuracy of 98.80% with an EER of 1.38. These results underscore the effectiveness of the ViT framework in achieving unprecedented accuracy and reliability for biometric authentication, making it a promising solution for secure and non-intrusive identification technologies.

Table III: Comparison of FPPBS with SOA Biometric systems; FSVP: Forehead Subcutaneous Vein Pattern, PBP: Periocular Biometric Pattern, IP: Iris Pattern, DHVP: Dorsal Hand Vein Pattern, FVP: Finger Vein Pattern, SRP: Sclera Recognition Pattern, FKP: Finger Knuckle Pattern, PPP: Palm print pattern, DPVM: Dynamic palm vein matching, HS: Hyperspectral, FS: Finger Shape.

Ref	Pattern	Database	Sam. (Sub.)	Feature Extracted	Classification	Accuracy	EER
[57]	PBP	IMP	62 (620)	PHOG	Neural Networks	75.48	3.50
[22]	FVP	FV-USM	492 (123)	DCNN	Softmax	69.33	0.80
	FVP	HKPU	302 (156)			84.59	2.33
[58]	FVP	FV-USM	492 (123)	BLPOC, WCCD	Score Level Fusion	-	2.34
[59]	DPVM	CASIA	200	RootSIFT	LBP-based mismatching removal	-	0.996
[42]	DPVM	PolyU	500	Discriminative LBP	Chi-Square Distance	95.59	0.08
[47]	DPVM	CASIA	200	Adaptive Gabor Filter	Normalised Hamming Filter	-	0.12
[60]	DPVM	PolyU	500	Wave Atom transform	Normalised Hamming Filter	95.26	1.98
[61]	IP+PBP	CSIP	2004 (50)	LBP, HOG, ULBP, GIST, SIFT, Iriscode	Chi-Square Distance, Distance-Ratio Based Scheme, Hamming Distance	93.50	15.50
[62]	SRP+PBP	UBIRIS-V1	1877	MLBP	Normalized Hamming Distance, Score level fusion	-	3.26
[63]	PPP+DHVP	HHUT	3000 (100)	DWT+IDWT	SVM	98.80	1.38
[64]	PPP+DHVP	NCUT+GPDS+XJTU	(420)	DCNN, BGM	Hamming Distance	-	0.33
[65]	FVP+FKP	SDUMLA-HMT	(106)	DCNN	Softmax	98.31	0.29
[66]	FV+FS	HKPolyU-DB	(600)	DenseNet-161	Softmax	-	0.05
[67]	FP+FVP+FKP	CAUC	(195)	Local Coding based CNN	Softmax	99.90	1.21
[11]	FSVP+PBP	FSVP-PBP	1600 (200)	DCNN	Softmax	98.60	0.08
[68]	FP+FVP	FVC-HKP	1800 (150)	FAB-Net	AEF-Net	98.84	0.17
[68]	FP+FVP	CAS-FVU	1960 (123)	FAB-Net	AEF-Net	99.17	0.11
[68]	FP+FVP	HDPR-310	(256)	FAB-Net	AEF-Net	98.67	0.14
	<b>FSVP+PBP</b>	<b>FSVP+PBP</b>	<b>8750 (350)</b>	<b>CS-ViT</b>	<b>Softmax</b>	<b>98.8</b>	<b>0.0102</b>

### G. Discussion on Deployment

The computational complexity of the proposed framework is compared with the state-of-the-art methods in terms of the floating point operations (FLOPs) and the number of trainable parameters in Table IV. The value of FLOPs for each model is calculated based on compute operations required for forward pass using the one batch of the dataset with the image size of  $3 \times 256 \times 256$ . Since the proposed framework is a dual architecture to handle the dual biometric traits simultaneously, the two forehead and the periocular portions are concatenated before feeding to the state-of-the-art models for fair comparison. It can be observed that the value of the FLOPs for the proposed model is the lowest, even though the number of trainable parameters for the GoogleNet, VPCFormer, and ResNet50 are lower compared to our model. The FLOPs for these models become higher because of the concatenated input of the dual biometric traits. Furthermore, the number of CS-Encoder layers in the proposed framework is 6, which is half of the 12 layers in the standard ViT model [25]. Also, the size of the embedding dimension is 512, instead of 768 in the standard ViT model [25]. Therefore, the proposed framework is a lightweight model with the best performance and the robust against illumination variation. The lowest EER and highest TAR justify the best reliability

of the authentication by the proposed framework. Therefore, the proposed framework can be a new benchmark for the real-time deployment of touchless biometric authentication.

Table IV: Comparing the FLOPs and the trainable parameters.

Method	FLOPs (Billion)	Parameter (Million)
VGG16 [21]	643.36	135.69
ResNet50 [55]	173.16	24.22
GoogleNet [56]	63.26	5.95
PV-CNN [9]	3442.34	59.35
2D-FV-ViT [25]	111.07	86.36
FV-LT [26]	42.53	31.60
VPCFormer [27]	26.92	21.72
ABLSTM-TSVT [28]	77.91	100.09
<b>CS-ViT (Proposed)</b>	<b>13.32</b>	<b>26.46</b>

## VI. CONCLUSIONS

In this paper, we introduced a novel CS-ViT framework for biometric authentication that utilizes the concept of POC to compute the attention score in a multihead cross-spectral attention mechanism. The proposed Phase-Only Correlation Cross-Spectral Attention (POC-CSA) mechanism effectively captures phase-based structural features from the two biometric traits, ensuring robustness against variations in illumination and magnitude. A key innovation of the proposed approach lies in the

ability of the POC-CSA mechanism to extract essential biometric features using the forehead and the periocular images for accurate and precise subject identification. Further, the proposed adaptive Tann-Triggs algorithm for preprocessing the NIR images enhances the reliability of the CS-ViT framework for biometric authentication. The evaluation of the proposed framework on the extended FSVP-PBP database having 350 subjects demonstrates its superiority over state-of-the-art algorithms. The remarkable performance of the proposed framework underscores its potential as a robust and reliable solution for non-intrusive and touchless identity verification. Our findings not only contribute to the advancement of biometric authentication technologies but also open avenues for further research in exploring the capabilities of cross-spectral vision transformers in other domains of pattern recognition and image analysis.

## REFERENCES

- [1] M. Gomez-Barrero, P. Drozdowski, C. Rathgeb, J. Patino, M. Todisco, A. Nautsch, N. Damer, J. Priesnitz, N. Evans, and C. Busch, "Biometrics in the era of covid-19: challenges and opportunities," *IEEE Transactions on Technology and Society*, vol. 3, no. 4, pp. 307–322, 2022.
- [2] Z. Wang, B. Huang, G. Wang, P. Yi, and K. Jiang, "Masked face recognition dataset and application," *IEEE Transactions on Biometrics, Behavior, and Identity Science*, vol. 5, no. 2, pp. 298–304, 2023.
- [3] A. Makrushin, A. Uhl, and J. Dittmann, "A survey on synthetic biometrics: Fingerprint, face, iris and vascular patterns," *IEEE Access*, vol. 11, pp. 33 887–33 899, 2023.
- [4] Z. He, T. Tan, Z. Sun, and X. Qiu, "Toward accurate and fast iris segmentation for iris biometrics," *IEEE Transactions on Pattern Analysis and Machine Intelligence*, vol. 31, no. 9, pp. 1670–1684, 2009.
- [5] S. Adamović, V. Mišković, N. Maček, M. Milosavljević, M. Šarac, M. Saračević, and M. Gnjatović, "An efficient novel approach for iris recognition based on stylometric features and machine learning techniques," *Future Generation Computer Systems*, vol. 107, pp. 144–157, 2020.
- [6] J.-C. Lee, "A novel biometric system based on palm vein image," *Pattern Recognition Letters*, vol. 33, no. 12, pp. 1520–1528, 2012.
- [7] S. Joardar, A. Chatterjee, and A. Rakshit, "A real-time palm dorsa subcutaneous vein pattern recognition system using collaborative representation-based classification," *IEEE Transactions on Instrumentation and Measurement*, vol. 64, no. 4, pp. 959–966, 2014.
- [8] J. E. S. Pascual, J. Uriarte-Antonio, R. Sanchez-Reillo, and M. G. Lorenz, "Capturing hand or wrist vein images for biometric authentication using low-cost devices," in *2010 Sixth International Conference on Intelligent Information Hiding and Multimedia Signal Processing*. IEEE, 2010, pp. 318–322.
- [9] R. Das, E. Piciuccio, E. Maiorana, and P. Campisi, "Convolutional neural network for finger-vein-based biometric identification," *IEEE Transactions on Information Forensics and Security*, vol. 14, no. 2, pp. 360–373, 2018.
- [10] S. Shekhar, V. M. Patel, N. M. Nasrabadi, and R. Chellappa, "Joint sparse representation for robust multimodal biometrics recognition," *IEEE Transactions on Pattern Analysis and Machine Intelligence*, vol. 36, no. 1, pp. 113–126, 2014.
- [11] S. Bhattacharya, A. Ranjan, and M. Reza, "A portable biometrics system based on forehead subcutaneous vein pattern and periocular biometric pattern," *IEEE Sensors Journal*, vol. 22, no. 7, pp. 7022–7033, 2022.
- [12] N. Miura, A. Nagasaka, and T. Miyatake, "Feature extraction of finger-vein patterns based on repeated line tracking and its application to personal identification," *Machine vision and applications*, vol. 15, pp. 194–203, 2004.
- [13] —, "Extraction of finger-vein patterns using maximum curvature points in image profiles," *IEICE TRANSACTIONS on Information and Systems*, vol. 90, no. 8, pp. 1185–1194, 2007.
- [14] W. Song, T. Kim, H. C. Kim, J. H. Choi, H.-J. Kong, and S.-R. Lee, "A finger-vein verification system using mean curvature," *Pattern Recognition Letters*, vol. 32, no. 11, pp. 1541–1547, 2011.
- [15] H. Zhang, Z. Liu, Q. Zhao, C. Zhang, and D. Fan, "Finger vein recognition based on gabor filter," in *Intelligence Science and Big Data Engineering: 4th International Conference, ISIDE 2013, Beijing, China, July 31–August 2, 2013, Revised Selected Papers 4*. Springer, 2013, pp. 827–834.
- [16] J. H. Choi, W. Song, T. Kim, S.-R. Lee, and H. C. Kim, "Finger vein extraction using gradient normalization and principal curvature," in *Image Processing: Machine Vision Applications II*, vol. 7251. SPIE, 2009, pp. 359–367.
- [17] W. Kang, "Vein pattern extraction based on vectorgrams of maximal intra-neighbor difference," *Pattern Recognition Letters*, vol. 33, no. 14, pp. 1916–1923, 2012.
- [18] S. A. Radzi, M. K. Hani, and R. Bakhteri, "Finger-vein biometric identification using convolutional neural network," *Turkish Journal of Electrical Engineering and Computer Sciences*, vol. 24, no. 3, pp. 1863–1878, 2016.
- [19] K. Itqan, A. Syafeeza, F. Gong, N. Mustafa, Y. Wong, and M. Ibrahim, "User identification system based on finger-vein patterns using convolutional neural network," *ARPJ Journal of Engineering and Applied Sciences*, vol. 11, no. 5, pp. 3316–3319, 2016.
- [20] J. Wang and G. Wang, "Hand-dorsa vein recognition with structure growing guided cnn," *Optik*, vol. 149, pp. 469–477, 2017.
- [21] K. Simonyan and A. Zisserman, "Very deep convolutional networks for large-scale image recognition," *arXiv preprint arXiv:1409.1556*, 2014.
- [22] H. Qin and M. A. El-Yacoubi, "Deep representation for finger-vein image-quality assessment," *IEEE Transactions on Circuits and Systems for Video Technology*, vol. 28, no. 8, pp. 1677–1693, 2017.
- [23] D. Zhong, S. Liu, W. Wang, and X. Du, "Palm vein recognition with deep hashing network," in *Pattern Recognition and Computer Vision: First Chinese Conference, PRCV 2018, Guangzhou, China, November 23–26, 2018, Proceedings, Part I 1*. Springer, 2018, pp. 38–49.
- [24] J. Wang, K. Yang, Z. Pan, G. Wang, M. Li, and Y. Li, "Minutiae-based weighting aggregation of deep convolutional features for vein recognition," *IEEE Access*, vol. 6, pp. 61 640–61 650, 2018.
- [25] X. Li and B.-B. Zhang, "Fv-vit: Vision transformer for finger vein recognition," *IEEE Access*, vol. 11, pp. 75 451–75 461, 2023.
- [26] H. Qin, R. Hu, M. A. El-Yacoubi, Y. Li, and X. Gao, "Local attention transformer-based full-view finger-vein identification,"

- IEEE Transactions on Circuits and Systems for Video Technology*, vol. 33, no. 6, pp. 2767–2782, 2023.
- [27] P. Zhao, Y. Song, S. Wang, J.-H. Xue, S. Zhao, Q. Liao, and W. Yang, “Vpcformer: A transformer-based multi-view finger vein recognition model and a new benchmark,” *Pattern Recognition*, vol. 148, p. 110170, 2024.
- [28] H. Qin, Z. Xiong, Y. Li, M. A. El-Yacoubi, and J. Wang, “Attention blstm-based temporal-spatial vein transformer for multi-view finger-vein recognition,” *IEEE Transactions on Information Forensics and Security*, vol. 19, pp. 9330–9343, 2024.
- [29] R. Albano, L. Giusti, E. Maiorana, and P. Campisi, “Explainable vision transformers for vein biometric recognition,” *IEEE Access*, 2024.
- [30] B. Huang, Y. Dai, R. Li, D. Tang, and W. Li, “Finger-vein authentication based on wide line detector and pattern normalization,” in *2010 20th international conference on pattern recognition*. IEEE, 2010, pp. 1269–1272.
- [31] M. A. Syarif, T. S. Ong, A. B. Teoh, and C. Tee, “Enhanced maximum curvature descriptors for finger vein verification,” *Multimedia Tools and Applications*, vol. 76, pp. 6859–6887, 2017.
- [32] P. Zhao, S. Zhao, J.-H. Xue, W. Yang, and Q. Liao, “The neglected background cues can facilitate finger vein recognition,” *Pattern Recognition*, vol. 136, p. 109199, 2023.
- [33] W. Yang, C. Hui, Z. Chen, J.-H. Xue, and Q. Liao, “Fv-gan: Finger vein representation using generative adversarial networks,” *IEEE Transactions on Information Forensics and Security*, vol. 14, no. 9, pp. 2512–2524, 2019.
- [34] Y. Song, P. Zhao, W. Yang, Q. Liao, and J. Zhou, “Eifnet: An explicit and implicit feature fusion network for finger vein verification,” *IEEE Transactions on Circuits and Systems for Video Technology*, vol. 33, no. 5, pp. 2520–2532, 2022.
- [35] A. Dosovitskiy, L. Beyer, A. Kolesnikov, D. Weissenborn, X. Zhai, T. Unterthiner, M. Dehghani, M. Minderer, G. Heigold, S. Gelly *et al.*, “An image is worth 16x16 words: Transformers for image recognition at scale,” *arXiv preprint arXiv:2010.11929*, 2020.
- [36] J. Huang, W. Luo, W. Yang, A. Zheng, F. Lian, and W. Kang, “Fvt: Finger vein transformer for authentication,” *IEEE Transactions on Instrumentation and Measurement*, vol. 71, pp. 1–13, 2022.
- [37] J. Rice, “Apparatus for the identification of individuals,” Oct. 13 1987, uS Patent 4,699,149.
- [38] J. Cross and C. Smith, “Thermographic imaging of the subcutaneous vascular network of the back of the hand for biometric identification,” in *Proceedings The Institute of Electrical and Electronics Engineers. 29th Annual 1995 International Carnahan Conference on Security Technology*. IEEE, 1995, pp. 20–35.
- [39] C.-L. Lin and K.-C. Fan, “Biometric verification using thermal images of palm-dorsa vein patterns,” *IEEE Transactions on Circuits and systems for Video Technology*, vol. 14, no. 2, pp. 199–213, 2004.
- [40] D. Huang, Y. Tang, Y. Wang, L. Chen, and Y. Wang, “Hand-dorsa vein recognition by matching local features of multisource keypoints,” *IEEE transactions on cybernetics*, vol. 45, no. 9, pp. 1823–1837, 2014.
- [41] X. Li, D. Huang, and Y. Wang, “Comparative study of deep learning methods on dorsal hand vein recognition,” in *Biometric Recognition: 11th Chinese Conference, CCBR 2016, Chengdu, China, October 14-16, 2016, Proceedings 11*. Springer, 2016, pp. 296–306.
- [42] J. Wang and G. Wang, “Quality-specific hand vein recognition system,” *IEEE Transactions on Information Forensics and Security*, vol. 12, no. 11, pp. 2599–2610, 2017.
- [43] P. Gupta and P. Gupta, “Multibiometric authentication system using slap fingerprints, palm dorsal vein, and hand geometry,” *IEEE Transactions on Industrial Electronics*, vol. 65, no. 12, pp. 9777–9784, 2018.
- [44] D. P. Egorov, P. V. Mizinov, O. V. Kravchenko, N. S. Konnova, and G. V. Osipenko, “Sift-based approach for dorsal hand veins images recognition,” in *2024 26th International Conference on Digital Signal Processing and its Applications (DSPA)*, 2024, pp. 1–4.
- [45] W. Kang and Q. Wu, “Contactless palm vein recognition using a mutual foreground-based local binary pattern,” *IEEE transactions on Information Forensics and Security*, vol. 9, no. 11, pp. 1974–1985, 2014.
- [46] Y.-P. Lee, “Palm vein recognition based on a modified,” *Signal, image and video processing*, vol. 9, no. 1, pp. 229–242, 2015.
- [47] X. Ma, X. Jing, H. Huang, Y. Cui, and J. Mu, “Palm vein recognition scheme based on an adaptive gabor filter,” *Iet Biometrics*, vol. 6, no. 5, pp. 325–333, 2017.
- [48] S. Bharathi and R. Sudhakar, “Biometric recognition using finger and palm vein images,” *Soft Computing*, vol. 23, no. 6, pp. 1843–1855, 2019.
- [49] S.-J. Horng, D.-T. Vu, T.-V. Nguyen, W. Zhou, and C.-T. Lin, “Recognizing palm vein in smartphones using rgb images,” *IEEE Transactions on Industrial Informatics*, vol. 18, no. 9, pp. 5992–6002, 2021.
- [50] A. Dosovitskiy, L. Beyer, A. Kolesnikov, D. Weissenborn, X. Zhai, T. Unterthiner, M. Dehghani, M. Minderer, G. Heigold, S. Gelly, J. Uszkoreit, and N. Houlsby, “An image is worth 16x16 words: Transformers for image recognition at scale,” 2021.
- [51] C. D. Kuglin, “The phase correlation image alignment method,” in *IEEE Int. Conf. on Cybernetics and Society, 1975*, 1975, pp. 163–165.
- [52] X. Tan and B. Triggs, “Enhanced local texture feature sets for face recognition under difficult lighting conditions,” *IEEE Transactions on Image Processing*, vol. 19, no. 6, pp. 1635–1650, 2010.
- [53] A. K. Sharma and N. K. Verma, “Quick learning mechanism with cross-domain adaptation for intelligent fault diagnosis,” *IEEE Transactions on Artificial Intelligence*, pp. 1–1, 2021.
- [54] K. Simonyan and A. Zisserman, “Very deep convolutional networks for large-scale image recognition,” 2015.
- [55] K. He, X. Zhang, S. Ren, and J. Sun, “Deep residual learning for image recognition,” in *2016 IEEE Conference on Computer Vision and Pattern Recognition (CVPR)*, 2016, pp. 770–778.
- [56] C. Szegedy, W. Liu, Y. Jia, P. Sermanet, S. Reed, D. Anguelov, D. Erhan, V. Vanhoucke, and A. Rabinovich, “Going deeper with convolutions,” in *Proceedings of the IEEE Conference on Computer Vision and Pattern Recognition (CVPR)*, 06 2015.
- [57] A. Sharma, S. Verma, M. Vatsa, and R. Singh, “On cross spectral periocular recognition,” in *2014 IEEE International Conference on Image Processing (ICIP)*. IEEE, 2014, pp. 5007–5011.
- [58] M. S. M. Asaari, S. A. Suandi, and B. A. Rosdi, “Fusion of band limited phase only correlation and width centroid contour distance for finger based biometrics,” *Expert Systems with Applications*, vol. 41, no. 7, pp. 3367–3382, 2014.
- [59] W. Kang, Y. Liu, Q. Wu, and X. Yue, “Contact-free palm-vein recognition based on local invariant features,” *PloS one*, vol. 9, no. 5, p. e97548, 2014.
- [60] F. Ahmad, L.-M. Cheng, and A. Khan, “Lightweight and privacy-preserving template generation for palm-vein-based human recognition,” *IEEE Transactions on Information Forensics and Security*, vol. 15, pp. 184–194, 2019.

- [61] G. Santos, E. Grancho, M. V. Bernardo, and P. T. Fiadeiro, "Fusing iris and periocular information for cross-sensor recognition," *Pattern Recognition Letters*, vol. 57, pp. 52–59, 2015.
- [62] K. Oh, B.-S. Oh, K.-A. Toh, W.-Y. Yau, and H.-L. Eng, "Combining sclera and periocular features for multi-modal identity verification," *Neurocomputing*, vol. 128, pp. 185–198, 2014.
- [63] C.-L. Lin, S.-H. Wang, H.-Y. Cheng, K.-C. Fan, W.-L. Hsu, and C.-R. Lai, "Bimodal biometric verification using the fusion of palmprint and infrared palm-dorsum vein images," *Sensors*, vol. 15, no. 12, pp. 31 339–31 361, 2015.
- [64] D. Zhong, H. Shao, and X. Du, "A hand-based multi-biometrics via deep hashing network and biometric graph matching," *IEEE Transactions on Information Forensics and Security*, vol. 14, no. 12, pp. 3140–3150, 2019.
- [65] S. Daas, A. Yahi, T. Bakir, M. Sedhane, M. Boughazi, and E.-B. Bourenane, "Multimodal biometric recognition systems using deep learning based on the finger vein and finger knuckle print fusion," *IET Image Processing*, vol. 14, no. 15, pp. 3859–3868, 2020.
- [66] K. J. Noh, J. Choi, J. S. Hong, and K. R. Park, "Finger-vein recognition based on densely connected convolutional network using score-level fusion with shape and texture images," *Ieee Access*, vol. 8, pp. 96 748–96 766, 2020.
- [67] S. Li, B. Zhang, S. Zhao, and J. Yang, "Local discriminant coding based convolutional feature representation for multimodal finger recognition," *Information Sciences*, vol. 547, pp. 1170–1181, 2021.
- [68] Y. Huang, H. Ma, and M. Wang, "Multimodal finger recognition based on asymmetric networks with fused similarity," *IEEE Access*, vol. 11, pp. 17 497–17 509, 2023.